Asian Journal of Physics

Volume 16 Numbers 2 & 3 April-September 2007

Special Issue on Space Weather

Guest Editors

P Janardhan, Hari Om Vats

K N Iyer, B G Anandarao

Asian Journal of Physics Vol.16, Nos. 2 & 3 (2007) 209-232

Insights from ground and space based observations of long lasting low density anomalies at 1 AU

P. Janardhan [1]
Physical Research Laboratory, Ahmedabad-380009, India, and
Instituto Nacional de Pesquisas Espaciais (INPE), Divisao de Astrofisica, Brazil
S. Ananthakrishnan
National Centre for Radio Astrophysics, TIFR, PO Box 3, Ganeshkhind, Pune, 411 007, India
V. Balasubramanian
Radio Astronomy Centre, TIFR, PO Box 8, Udaghamandalam (Ooty), 643 001, India

Abstract: The magnetic field in the heliosphere evolves in response to the photospheric field at its base. This evolution, together with the rotation of the Sun, drives space weather through the continually changing conditions of the solar wind and the magnetic field embedded within it. Given this broad framework, it appears that the solar sources of interplanetary disturbances that travel outwards from the Sun could be due to many causes. Although the majority of them could be due to CME's, there are many instances where they may have been caused by flare related events or transient coronal holes. It is apparent that all these phenomena are linked to the underlying disturbances in the magnetic field and that they manifest in different ways depending on the local conditions on the Sun. This paper will describe the efforts made with the Ooty Radio Telescope (ORT), since 1992, in making systematic interplanetary scintillation (IPS) observations of the solar wind with an aim to track traveling interplanetary disturbances and try and trace their solar sources. In particular, the paper will describe the insights gained from studies of long lasting ($\geq$ 24 hours) low density solar wind anomalies that have been observed at 1 AU.

1 Introduction

Understanding the nature and exact solar origins of sudden and intense geomagnetic activity on the earth has been a topic of current global research interest, with a number of spacecrafts like SOHO, YOHKOH and ACE devoting a large fraction of their time to this particular aspect. However, apart from space based platforms, ground based efforts involving interplanetary scintillation (IPS) measurements have also yielded important insights into solar wind processes [1-3] in the distance range 0.2-1.0 AU and have contributed in making systematic studies of the solar wind variations over the solar cycle [4-6]. In addition, IPS is the most cost effective method to study the large scale properties of the interplanetary medium from the ground. Though there is general consensus now that earth directed coronal mass ejections (CME's) are the major solar sources of intense geomagnetic storms [7], the debate is ongoing and the cause of such storms has been attributed, by different groups of research workers, to a variety of other solar surface features ranging from large solar flares and coronal holes to disappearing filaments and CME's [8,9].

[1]Corresponding author
email:jerry@prl.res.in; jerry@das.inpe.br

In an effort to study and understand this problem, extensive IPS observations have been carried out with the equatorially mounted Ooty Radio Telescope (ORT) which has a large effective collecting area of 8000 m^2 and is steerable in the East-West direction. Figure 1 is a picture of the large 530×30m Ooty Radio Telescope and Figure 2 shows an all sky map of the a grid of spatially well distributed compact extragalactic radio sources that were carefully selected from an extensive IPS sky survey, carried out between 1992 and 1994 with the ORT [10].

All the sources shown in Figure 2 are strong scintillators at 327 MHz and were used to study and track solar wind disturbances [11-13] between 0.2 and 1 AU. The thick curved line in the figure is the path of the Sun (ecliptic) through the sky. Using the ORT, density enhancements and solar wind velocities have been monitored in the directions of a large grid of compact extragalactic radio sources [10]. Having a known grid of compact scintillators in the sky enabled one to select and use the scintillating sources as a movable picket fence in the sky [12]. This method, coupled with simple theoretical model [14] enabled one to predict the approximate location, in space, of flare generated shocks and track, on a daily basis, traveling interplanetary disturbances from 0.2 to 0.8 AU [15]. Such tracking of interplanetary disturbances coupled with spacecraft data has been shown to be an efficient way of monitoring interplanetary transients and traveling interplanetary disturbances [16].

2 Interplanetary scintillation

Interplanetary scintillation arises, when electron density irregularities in the solar wind plasma scatter radio waves coming towards an observer from a distant radio source and produce random diffraction pattern on the ground resulting in intensity fluctuation of the radio source signal. Figure 3 shows a schematic of the observing geometry for a typical IPS observation. Letters 'S' and 'E' denote Sun and Earth. The line from 'E' through point 'P' is the line-of-sight (LOS) to a radio source respectively. The line from 'S' through 'P' refers to the radially directed solar wind across the LOS. The lines other than SE and SA are outside the ecliptic plane. The angles ϵ and γ are the solar elongation and heliographic latitude of the source.

The main parameters measurable by IPS are the scintillation index (m), a quantity that is proportional to the root mean square deviation in electron density, the scale size distribution of the density irregularities and the velocity of the solar wind. By definition, m is the ratio of the scintillating flux in a compact radio source to its mean source flux i.e $m = \Delta S / < S >$. For a given IPS observation m is simply the root mean-square deviation of the signal intensity to the mean signal intensity and can be easily determined from the power spectrum of the observed intensity fluctuations of compact extragalactic radio sources.

The ORT, with an effective collecting area of about 8000 m^2 and a declination (δ) coverage of -60° $\leq \delta \leq$ +60°, can observe 150–200 scintillating sources in the course of ten hours yielding high signal to noise ratio (S/N) power spectra with data stretches as short as two minutes. The spectra can be used to estimate the electron density fluctuations (ΔN_{rms}) in the solar wind and to derive the velocity of the solar wind across the LOS to the source [3,17,18]. At 327 MHz, the coverage in solar elongation (ϵ), which is the angle between the LOS to the source and the sun-earth line, is 15° $\leq \epsilon \leq$ 60°. This corresponds to $\sim 55 R_\odot \leq r \leq 190\ R_\odot$ where, r is the distance between the Sun and the LOS to the source and $R_\odot$ is the solar radius. Since the solar wind density may be taken as inversely proportional to r^2, measurements of scintillation index in the direction of a given radio source will drop off with increasing distance from the Sun. For an ideal point source, m will be unity just beyond the Fresnel distance at the observing wavelength λ and drop to values below unity with increasing distance r. The distance beyond the Fresnel zone, for the observing wavelength, is referred to as the weak scattering region wherein the total rms phase deviation imposed on a propagating plane wave from the radio source is much less than unity.

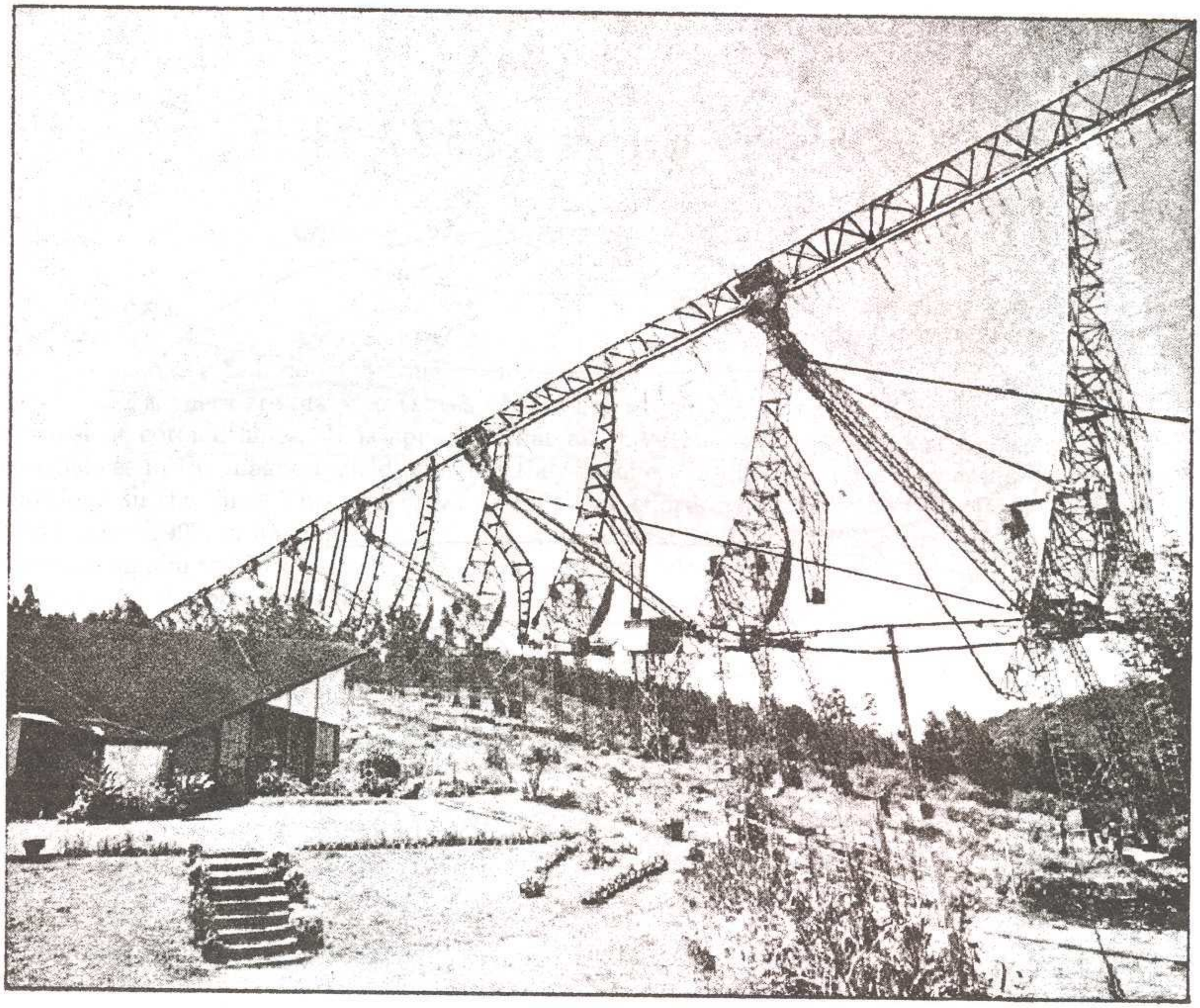

Figure 1: Shows a picture of the large, steerable, 530×30m (North-South×East-West) Ooty Radio Telescope (ORT) in South India that operates at 327 MHz.

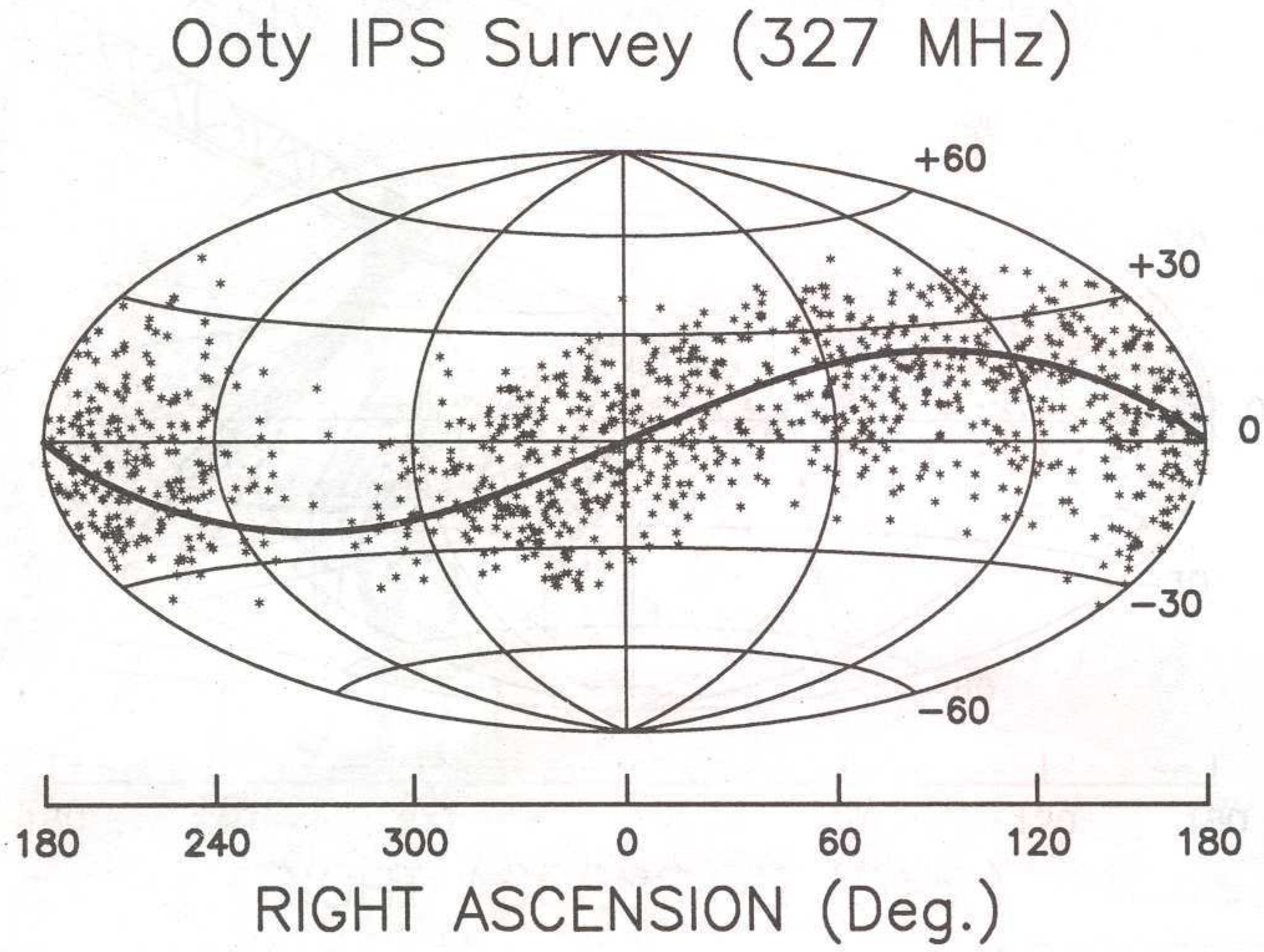

Figure 2: Shows an all sky map of the strong scintillators at 327 MHz. The curved black line is the path of the ecliptic through the sky.

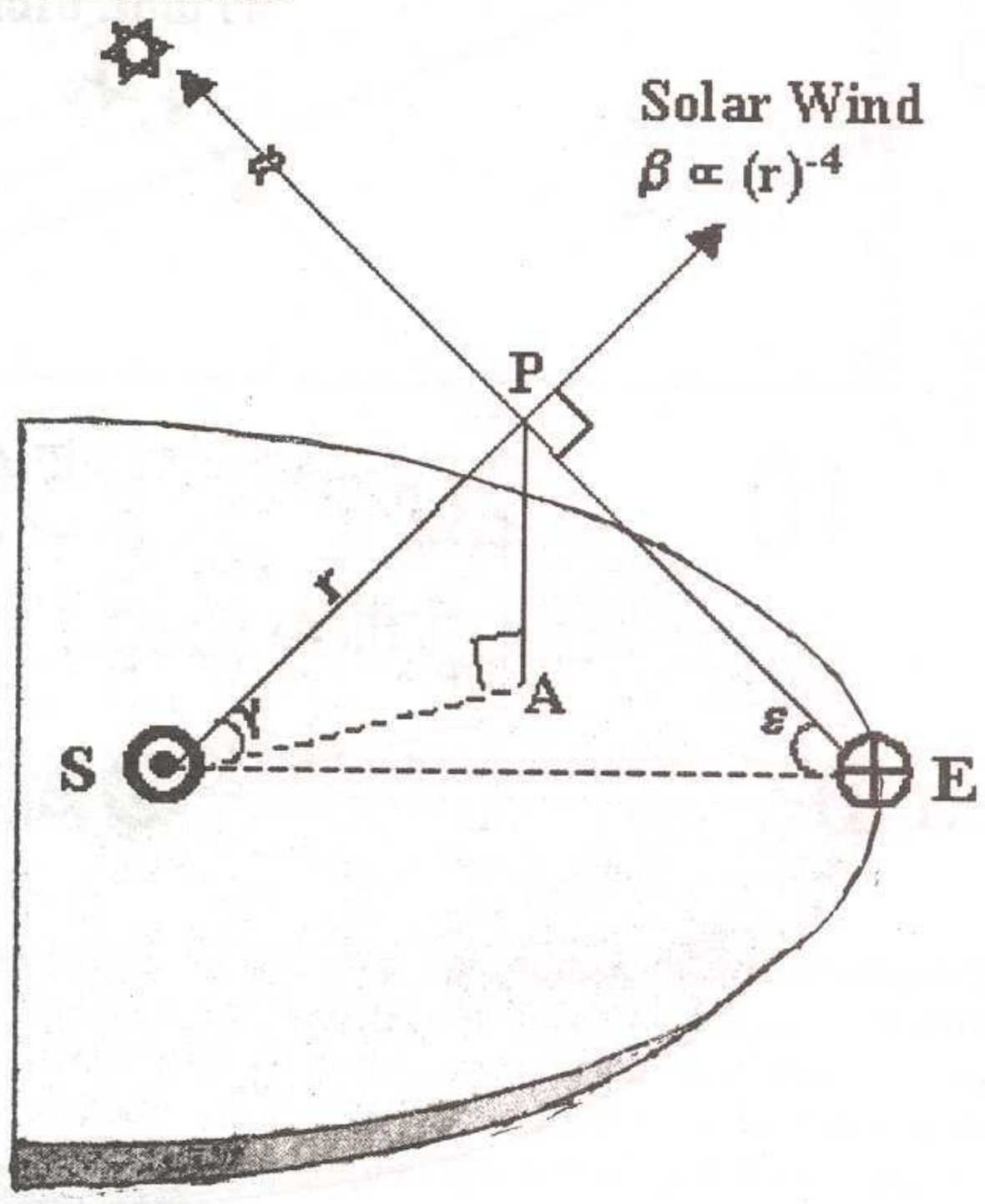

Figure 3: Shows a schematic of the observing geometry for a typical IPS observation with letters 'S', 'E' and 'P' denoting the Sun, earth and the closest point to the Sun along the LOS from the earth to the source. The lightly shaded semi-ellipse is the ecliptic plane with all lines other than SE and SA lying outside it. The line from 'S' through 'P' refers to the radially directed solar wind across the LOS. The angles ϵ and γ are the solar elongation and heliographic latitude, respectively.

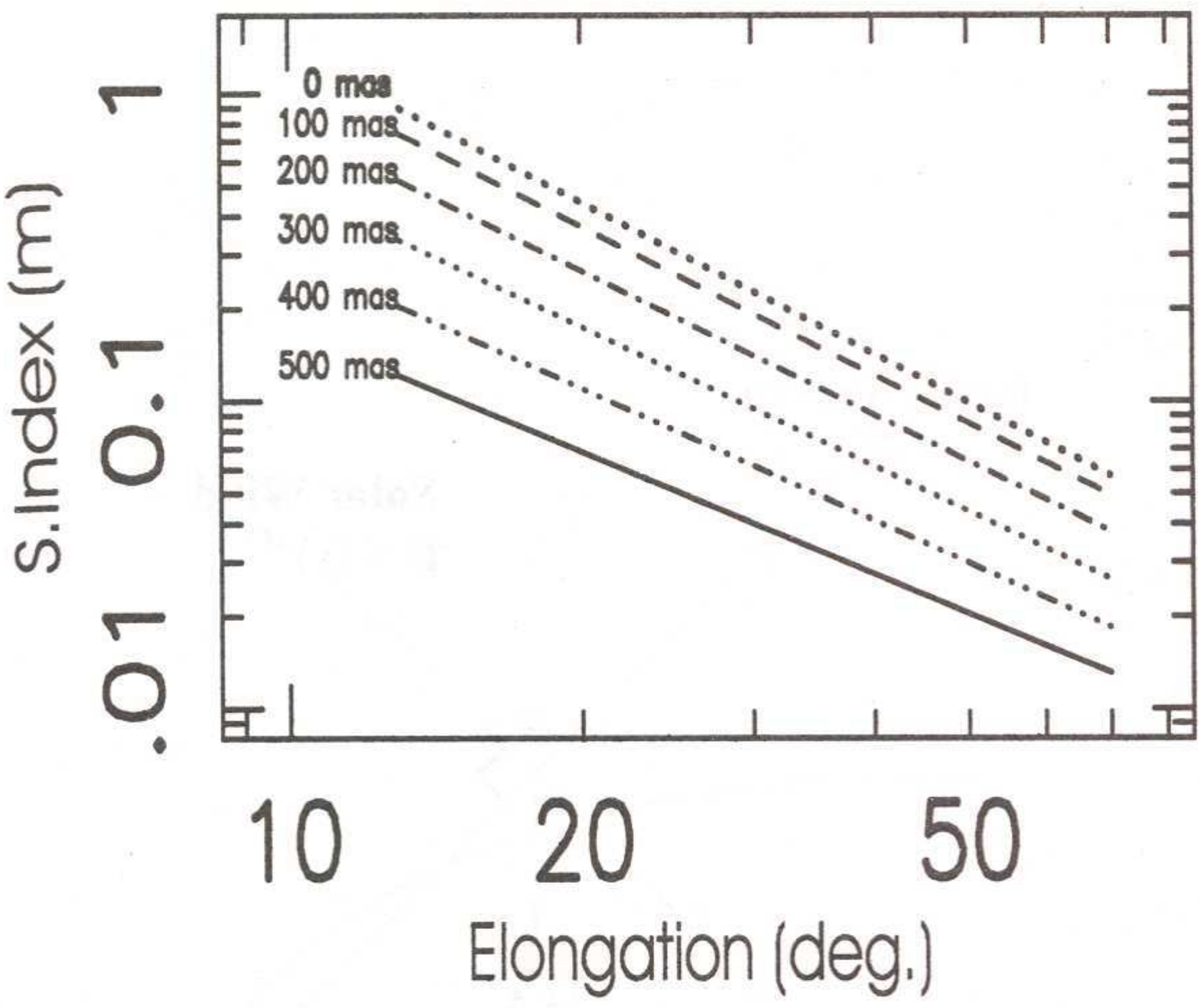

Figure 4: Shows the variation of scintillation index as a function of ϵ for different source sizes between 0 and 500 milli arc seconds (mas)

Theoretically expected scintillation indices can thus be computed by obtaining theoretical temporal power spectrum using a solar wind model, like the standard Marians Model [19], assuming weak scattering and a power law distribution of density irregularities in the interplanetary medium for any given source size and distance r of the LOS from the Sun, as defined by point 'P' on the LOS (see fig 3). Figure 4 shows the theoretically expected scintillation indices as a function of ϵ for various source sizes for weak scattering conditions at 327 MHz computed using the standard Marian's model calculations and assuming a power law index of 3.3. Curves for the variation of m versus solar distance (m-p curves) were computed for every source size between 0 and 500 milli arc seconds (mas) with ϵ varying from 15° to 70°.

Figure 5 shows actual observations (filled circles) of m as a function of elongation for several sources. The number of observations used, the IAU name of the source and the inferred angular source size in mas are indicated in each panel. The dashed straight line through the observed points in each panel are the theoretically computed behavior expected using Marian's model [19] for the source size indicated in each panel. Thus a comparison between actual observations of m with corresponding theoretical estimates for various source sizes and distances can yield estimates of the equivalent compact component size of the radio source. Alternatively, compact component sizes can also be derived by model fitting IPS power spectra. This method however requires IPS power spectra having S/N $\geq$25 db.

It must be emphasized that scintillation only measures the variation in density ΔN_{rms} and not directly the density N_e itself. A good proxy for the solar wind density can be obtained in terms

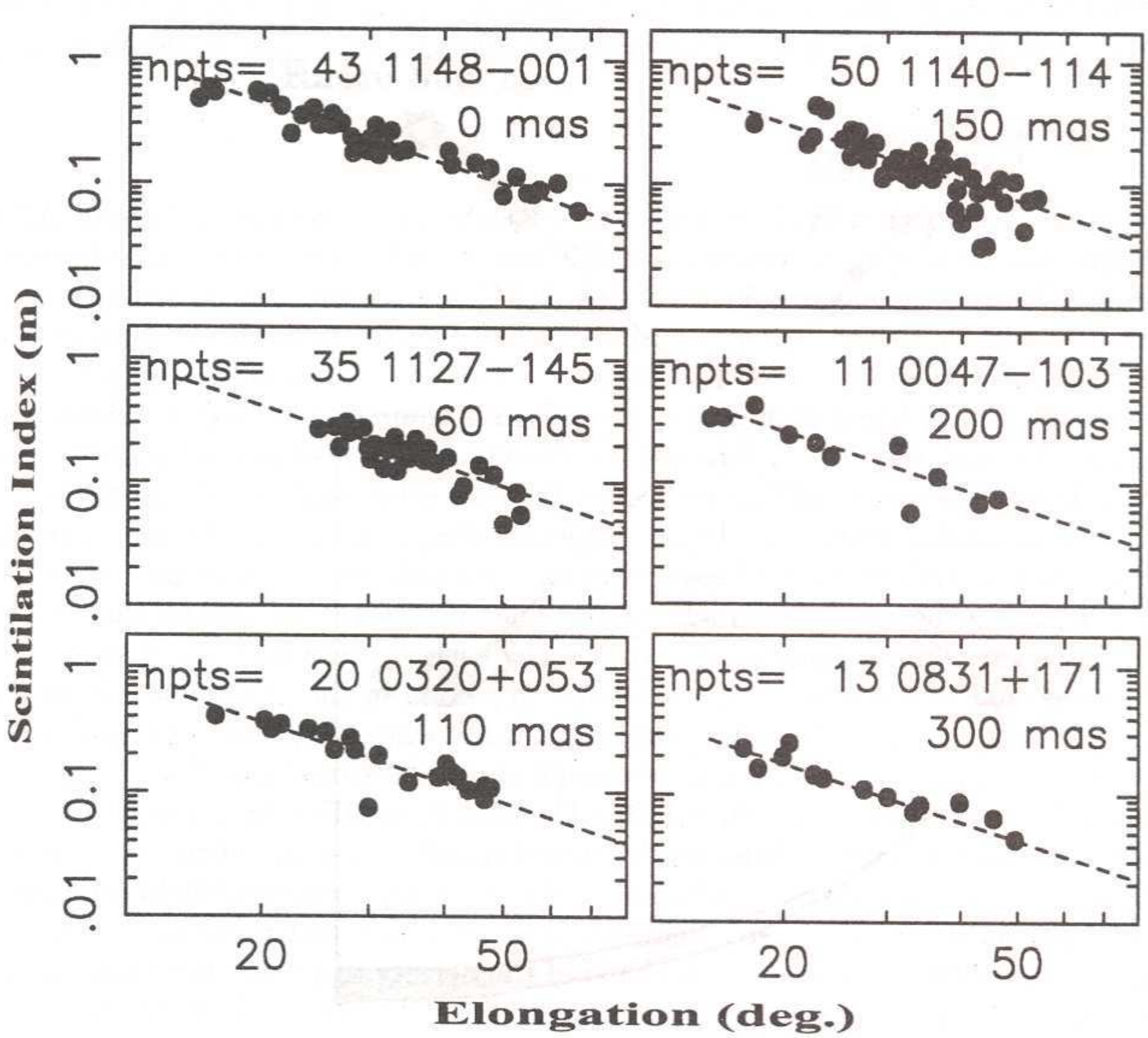

Figure 5: Shows the variation of scintillation index as a function of ϵ for different sources. The observed scintillation indices are shown by filled dots. The number of observations used, the IAU name of the source and the inferred source size in milli arc seconds (mas) are indicated in each panel. The dashed line through the points in each panel is the theoretically computed behavior expected for the source size indicated in each panel.

of the value of a normalized scintillation index (m) defined as, $g = m(\epsilon)_{obs}/m(\epsilon)_{exp.}$. Here $m(\epsilon)_{obs}$ is the observed scintillation index at a given ϵ while $m(\epsilon)_{exp.}$ is the expected long-term average m of the source at the same ϵ. Using a large data base of IPS observations obtained between 1978 and 1979, from Cambridge, UK, Hewish et al [8] showed that there was no evidence for enhanced or decreased scintillation that was not associated with corresponding variations in density. IPS can therefore be used with confidence to monitor plasma density, using the g-values as a proxy for the densities, along the LOS to a source even though it measures only the fluctuation in density and not the density itself. Thus, a g-value unity would imply that the solar wind density, at point P, along the LOS to the source was equal to the long term mean value expected from the solar wind at the observed ϵ, while g-values > 1 and < 1 would imply enhanced and depleted densities, respectively.

3 Unusual solar wind outflows

The solar wind at earth orbit (1 AU) is known to be strongly supersonic and super Alfvénic with Mach and Alfvén numbers being on average 12 and 9, respectively. Also, solar wind densities (average $\sim$10 cm^{-3}) and velocities (average $\sim$450 km s^{-1}) at 1 AU, are known to be inversely correlated with low velocities having higher than average densities and vice versa. However, on May 11 and 12 1999 the earth was engulfed by an unusually low density (< 0.1 cm^{-3}) and low-velocity (< 350 km s^{-1}) solar wind with an Alfvén Mach number significantly less than 1. This was a unique low velocity, low density, sub-Alfvénic solar wind flow, which spacecraft observations have shown lasted more than 24 hours. One consequence of this extremely tenuous solar wind was a spectacular expansion of the earth's magnetosphere and bow shock. The expanding bow shock, which is normally located 10 earth radii, was observed by several spacecraft and reached record upstream distances of nearly 60 earth radii, equal to the size of the lunar orbit. The event was so dramatic that it has come to be known as the 'solar wind disappearance event'. The earliest reported case of such unusual solar wind outflows was that of the long duration density depletion in the interplanetary medium which was observed by Helios 1 and Helios 2 spacecraft in 1979 when they were 0.3 and 0.37 AU from the Sun [20]. Schwenn [21] reported "strange though rare excursions from the average solar wind" that occurred in November 1979, and June 1980. The data from HELIOS 1 during 6 to 8 June 1980 were dramatic because the proton densities decreased steadily over an entire day from the normal value of 100 cm^{-3} to less than 1 cm^{-3}, while the velocity and the magnetic field remained constant at 300 km s^{-1} and 35 nT, respectively. Schwenn [21] has noted that there was no disturbance in the interplanetary medium for several days ahead of the density drop, nor was there any associable solar surface feature. Solar Geophysical Data reports during the period December 1979–July 1980 showed that a solar polar field reversal had taken place.

The extremely spectacular nature of the 'solar wind disappearance event' of 11 May 1999 has caused it to be one of the most extensively studied and reported solar wind related events in recent times. A number of observations have been reported using both space based and ground based instrumentation [22-28]. Using archival data [24] reported on the solar-cycle variation of low density solar wind during more than three solar cycles using the the OMNI near-earth solar wind density data in the period 1965-1999. The authors concluded that low density periods were accompanied by low mass fluxes and dynamic pressures. They found that approximately two-thirds of the events having densities < 1 cm^{-3}, were associated with transient solar wind structures, like for example CME ejecta where the low densities may arise from the expansion of the low density plasma in the dim core of CMEs observed by coronagraphs. Around a quarter of all low density events in this data set were found to occur in co-rotating high-speed streams, an association that is not unexpected since in general faster solar wind speeds have lower densities. However, the May 1999 low density event was unusual in that it was not clearly associated with an ejecta or a co-rotating stream. Richardson

et al [24] also reported that low density plasma was apparently observed more frequently around the maximum of solar cycles 20 and 23, both of which were weaker cycles compared to cycles 21 and 22. They thus concluded that low density events may be a more prominent feature of weaker solar cycles.

In another independent study [29], the OMNI and ACE spacecraft databases from 1962 to 2002 were used to select those events that have densities of ≤ 0.4 cm^{-3}. A total of 18 such events were found of which seven, including the 11 May 1999 event during Carrington Rotation 1949 (CR1949), were found to have minimum density values of ≤ 0.2 cm^{-3} and Table 1 shows these seven events [29]. It can be seen from Table 1 that the Alfvén Mach numbers (last column) are all significantly less than 1. It may also be noted that the values of ρ_{min} and Alfvén Mach No. for the 11 May event are significantly lower than any of the other events listed. Since all seven events listed in Table 1 took place close to the solar maximum and since the solar polar field undergoes a reversal at each maximum, it was speculated [25,27,29] that the large scale restructuring of the solar magnetic fields accompanied by the deformation of the heliospheric current sheet that takes place at the beginning of any solar activity cycle, is likely to be associated with density anomalies.

Table 1. Disappearance Events.

Date	Day No.	Rotation	ρ_{min} (cm^{-3})	Alfvén Mach No.
18-10-77	293	1660	0.20	0.79
04-07-79	185	1683	0.10	0.61
31-07-79	212	1684	0.20	0.68
22-11-79	326	1688	0.10	0.54
11-05-99	131	1949	0.02	0.41
20-03-02	79	1987	0.14	0.50
24-05-02	144	1990	0.07	0.54

4 IPS Observations with the ORT

Using a set of around 150 strong scintillators, a large part of the inner heliosphere at southern declinations between 0.2 and 0.9 AU was monitored using the ORT. IPS observations were obtained, on a daily basis, between 3–16 May 1999. It was immediately apparent from the data that solar wind conditions during the period were unusual because the scintillation levels for all the sources were much below normal implying that large portions of the interplanetary medium were experiencing unusually low densities. Under normal solar wind conditions, one would expect the general scatter in the g-values to be around a mean g of unity. Figure 6 shows the distribution of g-values plotted as histograms for each day of observations.

The date and number of sources observed is indicated in each panel.The histograms indicate that the entire interplanetary medium (IPM) was experiencing lower than normal densities thereby implying that the micro-turbulence [30] in the interplanetary medium remained low for a prolonged duration of several days over a large part of the inner heliosphere. The IPS observations also showed several LOS where the g-values dropped very steeply in a manner similar to that seen by spacecraft. The left hand panel of Figure 7 shows hourly averaged values of proton densities (filled dots) as a function of date in May 1999 (data available at *http* :

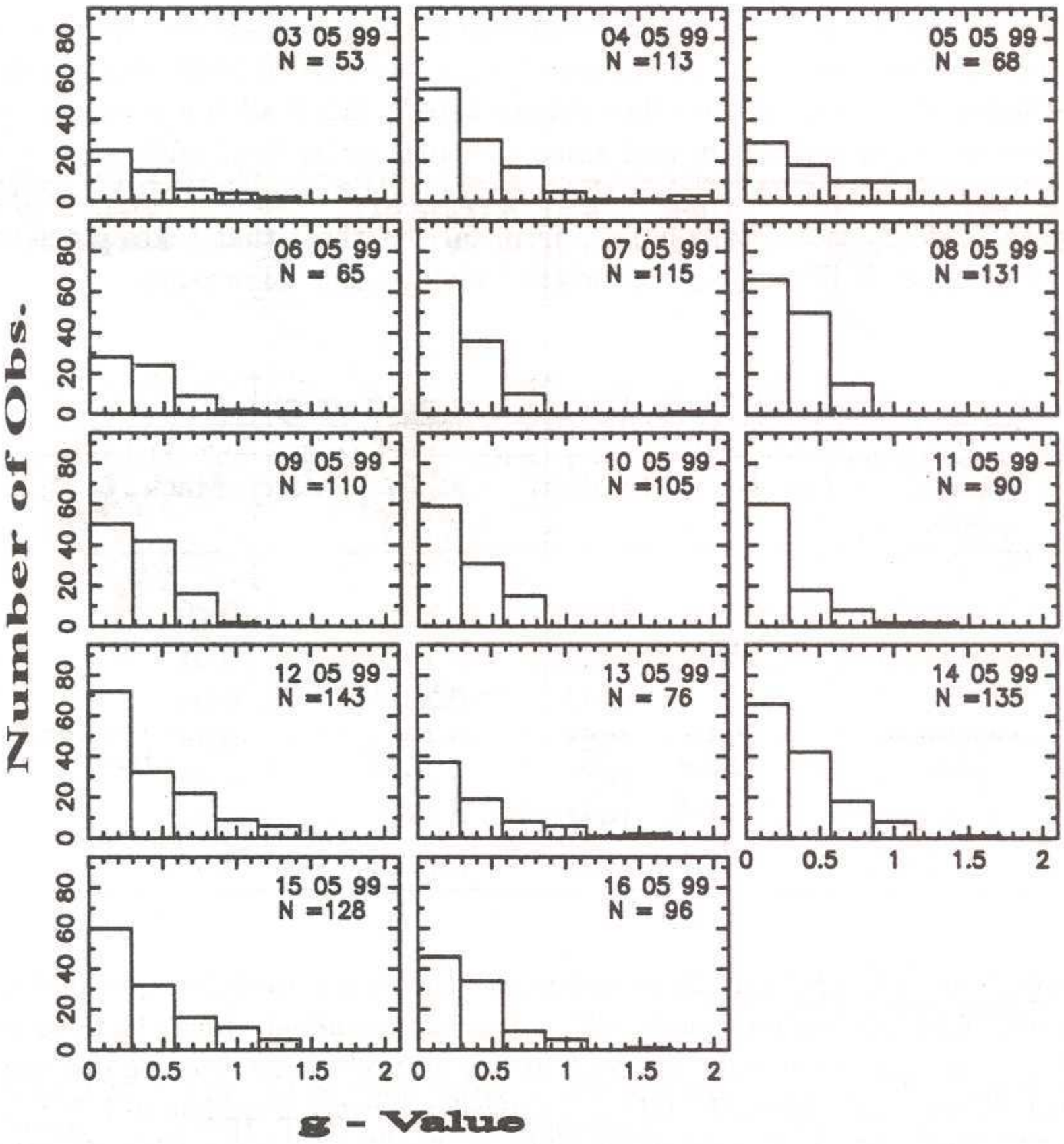

Figure 6: Shows histograms of g-values for each day of observation. Note that most of the observations on all days have g < 1. The histogram for 11 May 1999 clearly shows a much steeper drop in densities with around 95% of the sources being observed with g-values less than 0.6. The number of sources observed each day is indicated in each panel.

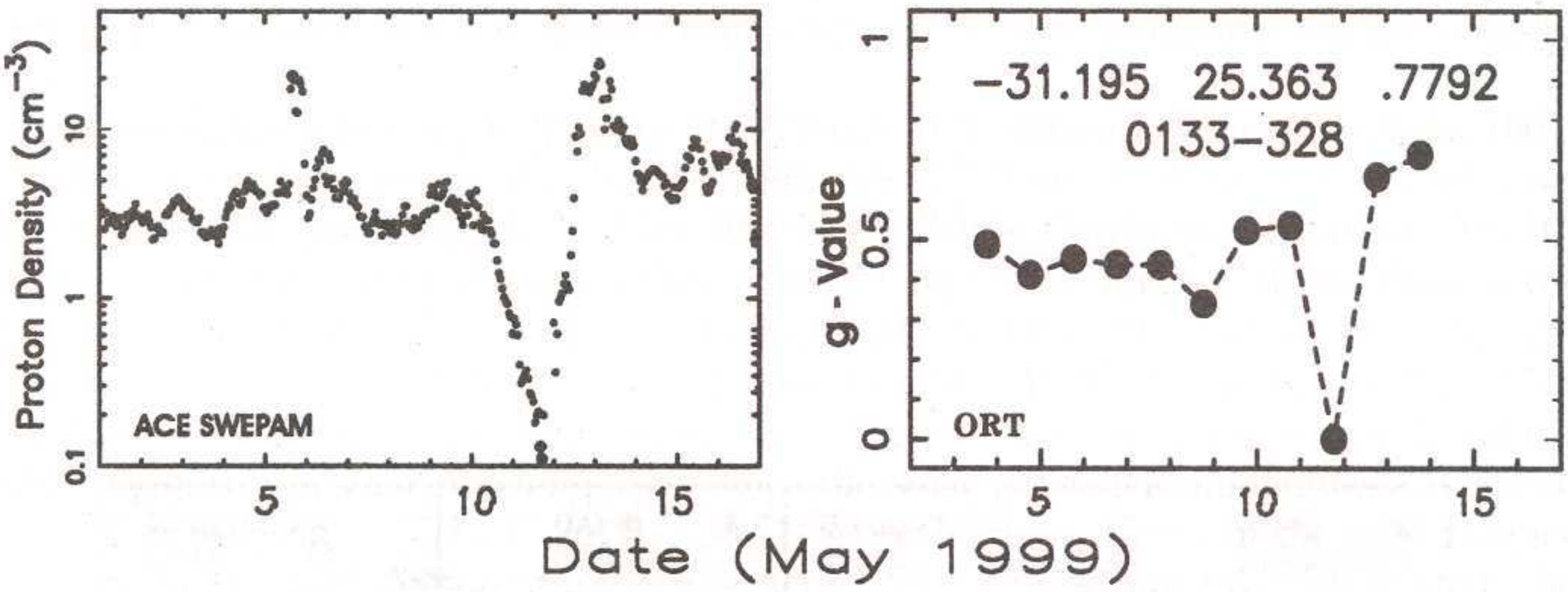

Figure 7: Shows measurements of proton densities from the SWEPAM instrument onboard the ACE spacecraft (left panel) and a single example of IPS observations of g-values versus date of observation (right panel) for a source that showed a clear dip in g-values on and around the 11th May 1999. The helio latitude, helio longitude, distance from the Sun in AU and source name are shown at the top of each panel.

//www.srl.caltech.edu/ACE/ASC/level2/lvl2DATA_SWEPAM.html) as seen by the SWEPAM instrument onboard the ACE spacecraft while the right hand panel shows an example of IPS measurements of g-value (filled dots joined by a dashed line) as a function of date in May 1999.

The heliographic coordinates of the observed source, distance from the LOS from the Sun in AU and the IAU name of the source are also indicated in the right hand panel. Figure 8 (left hand panel) shows a polar plot of g-values on 11 May 1999. The finely dotted circles are contours of equal ϵ with the Sun at the center. The various ranges of g-values are shown by different symbols with open five-pointed stars indicating $g = 0$; filled gray dots indicating $0.0 < g \leq 0.6$; open circles indicating $0.6 < g \leq 1.0$; and open squares indicating $g > 1.0$. It may be emphasized again that $g = 1$ implies that the solar wind densities are normal, while $g < 1$ and $g > 1$ imply depleted and enhanced densities, respectively. A similar polar plot is shown in the right hand panel for all the sources that showed a behaviour similar to that shown in the right hand panel of Figure 7. The g-values for each of the sources have been plotted for all those days it was observed, with the filled dots indicating g-values that became immeasurably low on or around 11 May 1999; gray crosses $0.0 < g \leq 0.6$; thick dashes $0.6 < g \leq 1.0$; and open circles indicating $g > 1.0$. It may be noted that g-values of sources adjacent to those represented by filled dots are by and large very low ($g \leq 0.6$). The right hand panel thus essentially represents the morphology of the large void that engulfed the earth on 11-12 May 1999 and it has been described as a "void-in-void" morphology by Balasubramanian et al [27].

4.1 The disappearance event of May 1999

An important aspect of the disappearance event of 11 May 1999 was that the solar wind flows were highly non-radial [28]. ACE measurements have shown that the deviations from radial flow of the solar wind on Day of Year (DOY) 131, was such that the azimuthal component of the solar wind velocity went as high as 100 km s^{-1}. Figure 9 shows hourly averaged values of ACE measurements of proton densities as a function of Azimuthal component of solar wind velocities on DOY 130-131

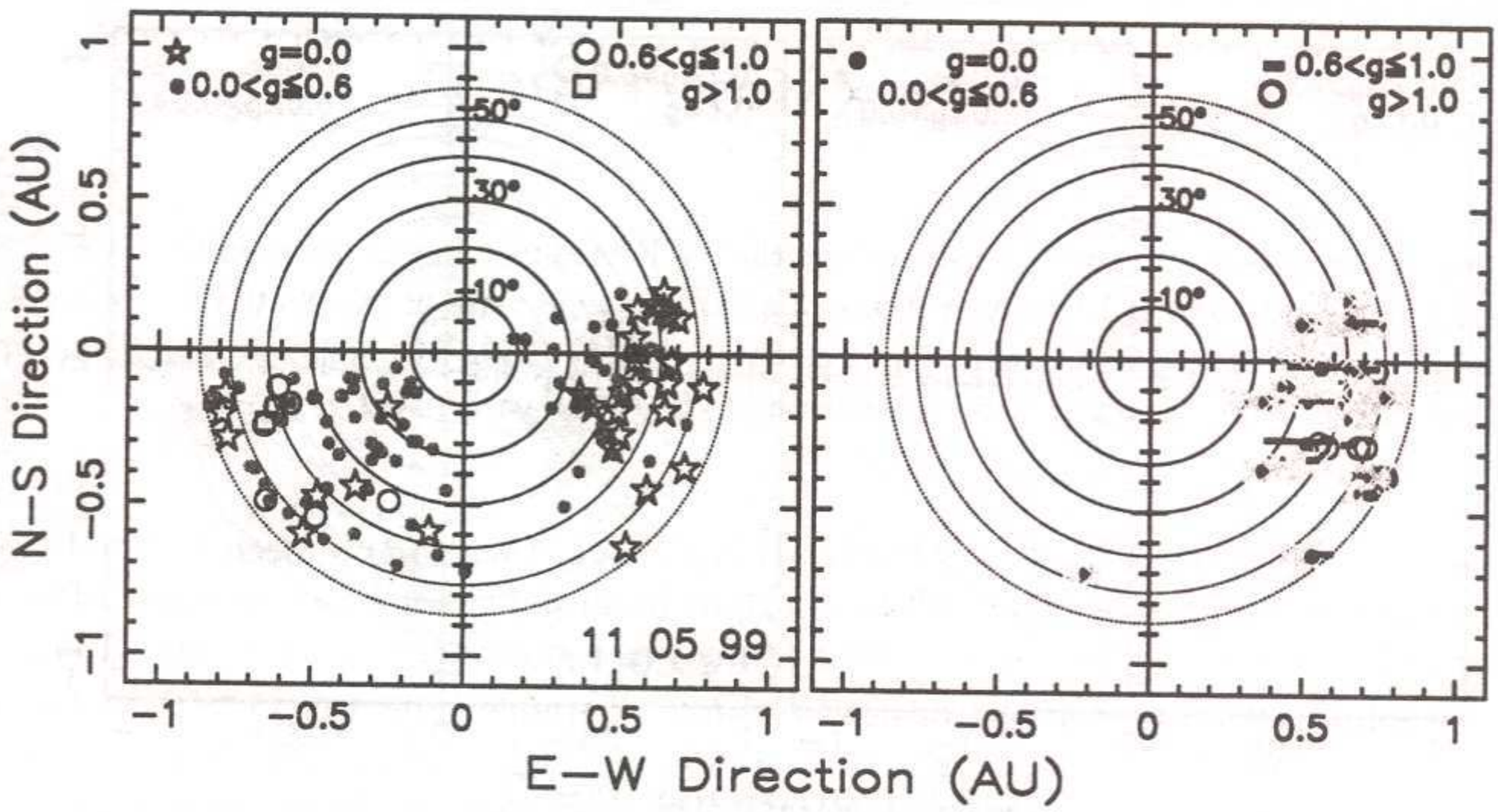

Figure 8: The left hand panel shows a polar plot of g-values on 11 May 1999. The finely dotted circles in both panels are circles of equal ϵ with the Sun at the center. The various ranges of g-values are shown by different symbols with open five-pointed stars indicating $g = 0$; filled gray dots indicating $0.0 < g \leq 0.6$; open circles indicating $0.6 < g \leq 1.0$; and open squares indicating $g > 1.0$. The right hand panel shows a polar plot of g-values for sources that showed a steep drop in g-values on and around 11 May 1999. The g-values for each of the sources have been plotted for all of the days it was observed. In the right hand panel, the filled dots indicate g-values that became immeasurably low on or around 11 May 1999. The gray crosses indicate $0.0 < g \leq 0.6$; thick dashes indicate $0.6 < g \leq 1.0$; and open circles indicate $g > 1.0$.

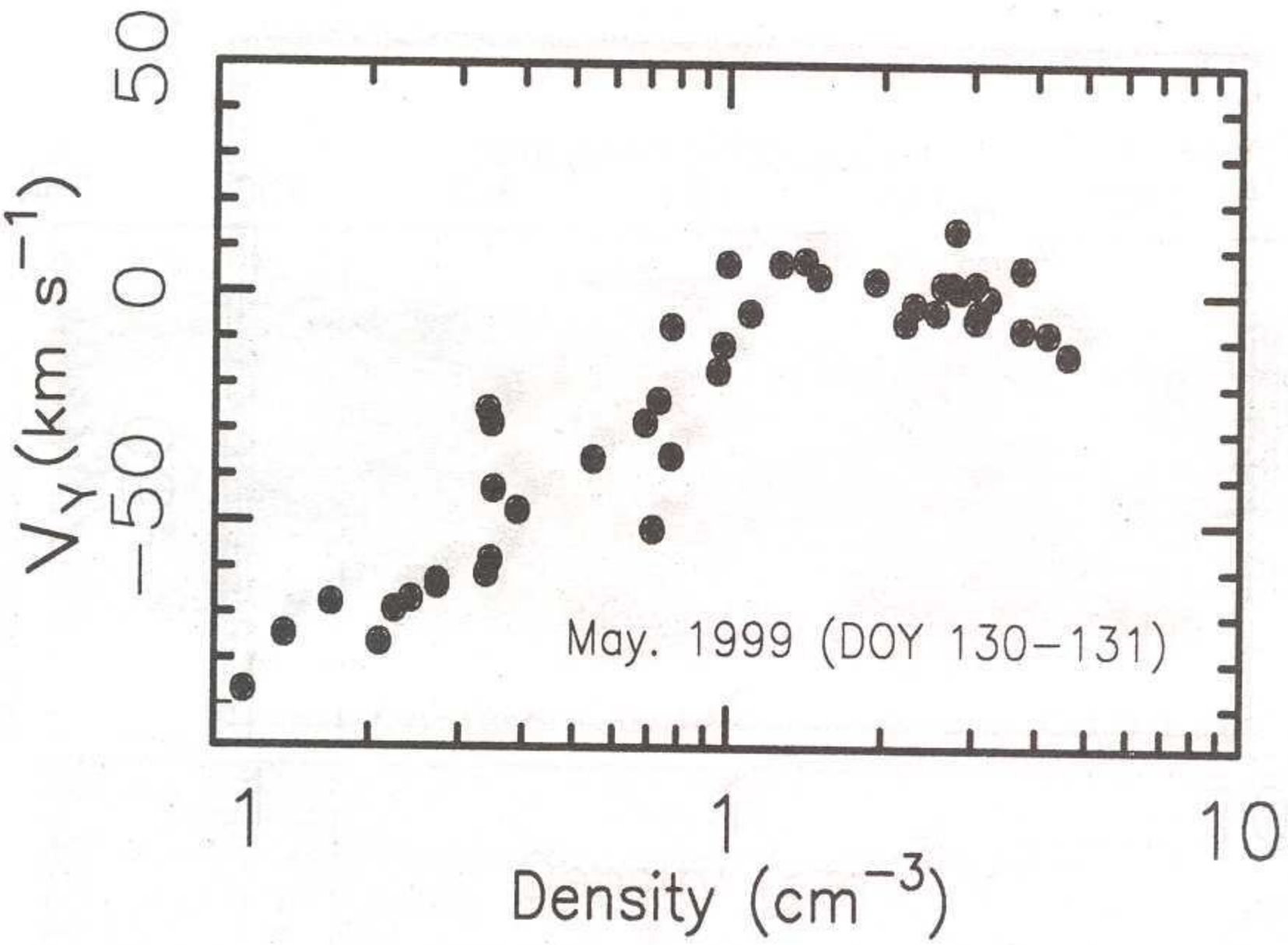

Figure 9: Shows hourly averages of the variation of proton density as a function of the azimuthal component of the solar wind velocity for two days (DOY 130-131) during the disappearance event of May 1999.

during the disappearance event of May 1999.

A clear anti-correlation can be seen with westward flow velocities increasing with decreasing densities. This clearly implies that the Alfvén radius, R_A (the distance to which the solar wind co-rotates with the Sun) which is normally a function of both the density and the magnetic field became independent of the magnetic field during this event, thus causing the Alfvén radius to extend outward by a factor of $\sim$5 times from its normal distance. Solar source locations are usually determined by tracing solar wind velocities back to the Sun along Archimedean spirals. However, under circumstances when the solar wind flows are highly non-radial, solar source locations computed by a trace-back technique using constant velocities along Archimedean spirals would be expected to have large errors. In a detailed and careful study of the disappearance event of 11 May 1999, the complicated process of tracking the interplanetary event back to the Sun has been carried out and using the fact that the Alfvén radius became independent of magnetic field, as shown above, it was shown that the traceback errors were not significant [28]. The upper panel of Figure 10 shows a tomographic synoptic velocity map for CR1949 in May 1999 made using IPS observations from the Solar Terrestrial Environment Laboratory (STEL), Toyokawa, Japan. Heliographic longitude is marked at the top of the panel. The upper panel demarcates, by dashed white lines, the locations of the stable, large scale, slow speed flows, < 400 km s^{-1}. The coronal hole boundaries are demarcated by dashed black lines. The path of the ACE spacecraft is shown, in the upper panel, by a thick black line along the equator. The lower panel shows a magnetogram from the SOHO spacecrafts MDI instrument. Central meridian passage (CMP) dates are marked at the bottom of the lower panel. Regions of large magnetic field strength, corresponding to active region locations are shown as black and white patches to distinguish the two magnetic polarities. The curved solid line, in the

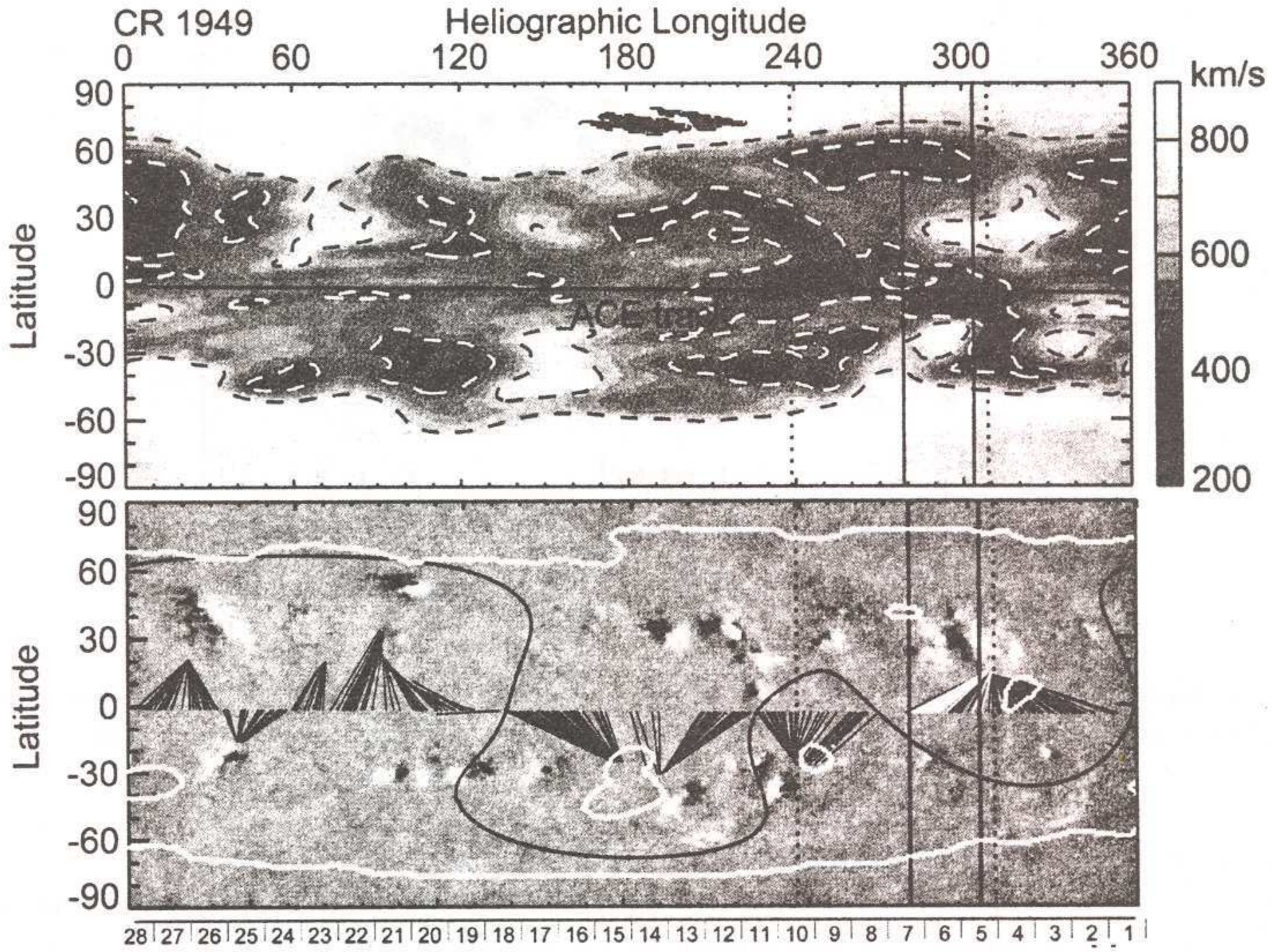

Figure 10: The upper panel shows a tomographic synoptic IPS velocity map during CR1949 in May 1999. The velocities are shown projected on the source surface at 2.5 $R_\odot$. The dashed white and black lines demarcate, respectively, the boundaries of the low velocity flows and polar coronal hole boundaries. The path of the ACE spacecraft is indicated by a thick line along the equator. The lower panel shows a synoptic map made using magnetograms from the MDI instrument on board the SOHO spacecraft. Regions of large magnetic field strength, corresponding to active region locations, are shown as black and white patches to distinguish the two magnetic polarities. The curved solid line, is the magnetic neutral line. Potential field computations of the magnetic fields are shown by converging black lines on the map that join magnetic fields on the source surface at 2.5 $R_\odot$ with their corresponding counterparts on the photosphere. The potential field lines that are marked in white correspond to fields with central meridian passage date of 11 May 1999. The two sets of solid and dashed vertical parallel lines running across all the panels demarcate, respectively, the back projected location of DOY 131 when the solar wind flow was highly non-radial and days on either side of DOY 131 when the solar wind flow was radial. Shown by thick white lines, in the lower panel are the locations of CH boundaries.

lower panel, is the magnetic neutral line. Converging black lines on the map join magnetic fields on the source surface at $2.5R_\odot$, derived from potential field computations [31], with their corresponding counterparts on the photosphere. The potential field lines that are marked in white correspond to fields with CMP date of 11 May 1999. The two sets of solid and dashed vertical parallel lines running across both the panels demarcate respectively, the back projected location of DOY 131 when the solar wind flow was highly non-radial and days on either side of DOY 131 when the solar wind flow was radial. The dashed vertically oriented parallel lines therefore represent the maximum possible errors in the back projected solar source locations. Shown by thick white lines, in the lower panel are the locations of the coronal hole boundaries as inferred from HeI 10830Å observations. The location of the small mid-latitude coronal hole at around $\sim 320^\circ$ close to the location of the large active region complex AR8525 points strongly towards a coronal hole origin of the solar wind flows of 11 May 1999. Further support for a coronal hole origin of the solar wind flows comes from the fact that the magnetic field during this period was both stable and unipolar. Figure 11 shows the magnitude of the magnetic field (upper panel) as a function of DOY, the direction of the field (middle panel); and the charge state ratio O^{7+}/O^{6+} (lower panel). One can see that the field shows hardly any fluctuations during DOY 131 and remains constant, the direction of the field remains unchanged in contrast to other days when the direction of the field shows large and rapid changes and the charge state ratio remains well below 0.2 on all days between 5–10 May 1999. In a detailed study of solar wind outflows from active region sources and coronal holes, it has been shown that solar wind from active region have higher ratios of O^{7+}/O^{6+}, than wind from coronal hole sources [32]. Wind from the active region sources typically had the ratio $O^{7+}/O^{6+} = 0.1$–0.6 (corresponding to an equilibrium oxygen freezing-in temperature range of $T_0 = 1.4$–1.9 MK) while coronal hole wind typically had $O^{7+}/O^{6+} < 0.2$, corresponding to $T_0 < 1.6$ MK. The low variance in the magnitude of the magnetic field, the lack of change in the actual direction of the magnetic field and the O^{7+}/O^{6+} ratios < 0.2 strongly support a coronal hole origin of the solar wind outflows responsible for the flows of 11 May 1999.

5 The disappearance events of March and May 2002

Of the three disappearance events that took place in solar cycle 23, two happened place in March and May 2002 during Carrington Rotations CR1987 and CR1990, respectively. It is instructive to compare these two events with that of 11 May 1999. Figure 12 shows the variation of the azimuthal component of the solar wind velocity, in the ecliptic plane, as a function of density for the disappearance events of March 2002 (left) and May 2002 (right). The densities and velocities are hourly averages measured by the ACE SWEPAM instrument onboard the SOHO spacecraft. It is clear from Figure 12 that as the density decreases, the azimuthal or westward flow deviation of the solar wind increases. This anti-correlation is most apparent in the data of 11 May 1999 (Fig. 9) and implies that, during both the disappearance events in March 2002 and May 2002, respectively, the Alfvén radius became independent of magnetic field in a manner similar to that of the disappearance event of May 1999. It is also clear from Figure 12 that, the solar wind flows at 1 AU were highly non-radial, with the azimuthal flow velocities going as high as 50 km s^{-1} and 80 km s^{-1} for the events of March and May 2002, respectively. Figure 13 shows, at 1 AU, the absolute magnitude of the interplanetary magnetic field (IMF) in nT for the events of March and May 2002 (top left and top right, respectively). The actual direction of the magnetic field in the ecliptic plane as a function of DOY in 2002 is shown for the events of March and May 2002 in the bottom left and bottom right panels, respectively. The vertically oriented dashed parallel lines demarcate DOY 79 (left hand panels) and DOY 144 (right hand panels) for the disappearance events of March and May 2002, respectively. It can be seen from Fig 13 that the magnetic field shows a low variance and is

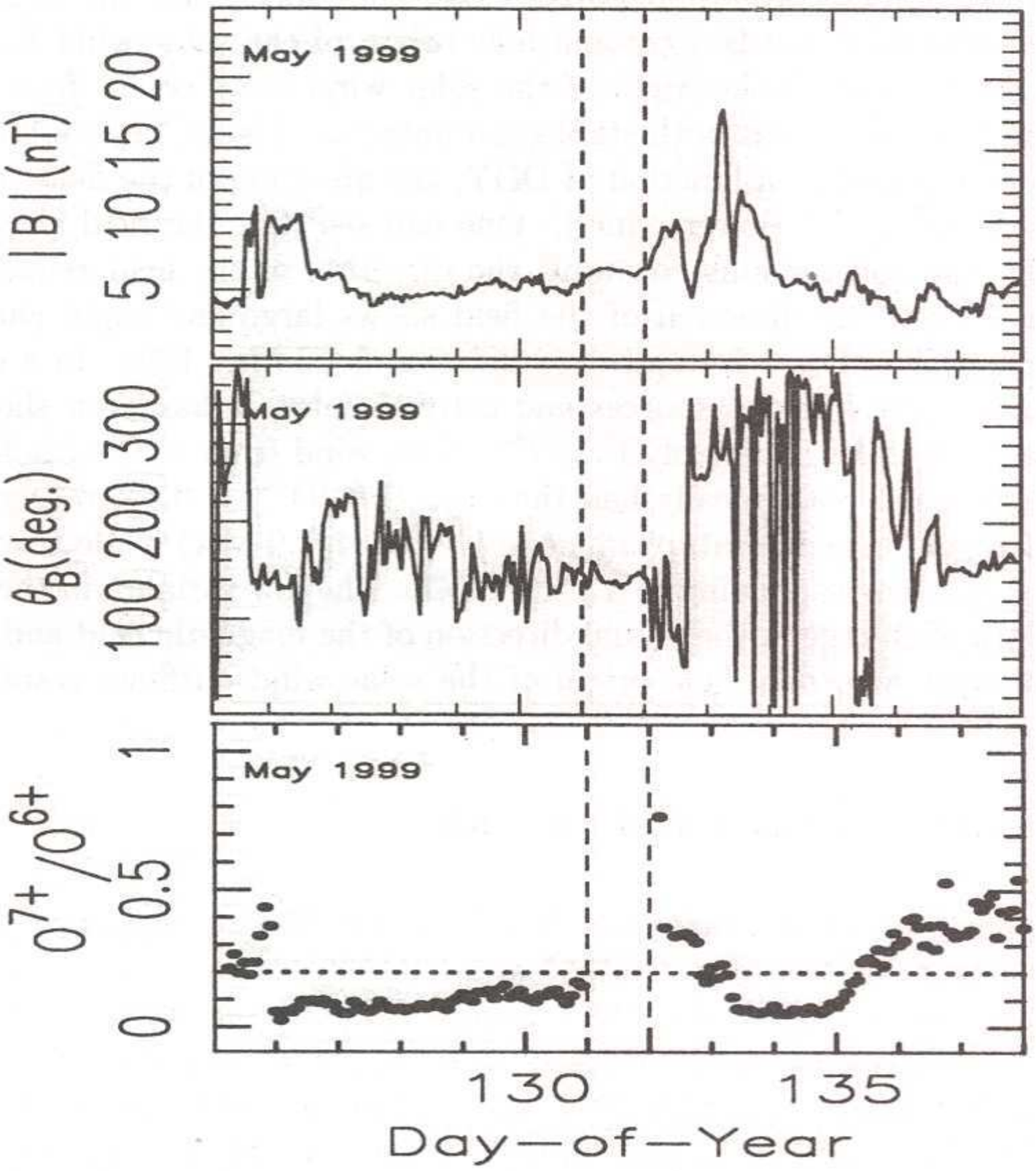

Figure 11: Shows as a function of DOY, the magnitude of the magnetic field (upper panel); the actual direction of the magnetic field (middle panel); and the charge state ratio O^{7+}/O^{6+} (lower panel)

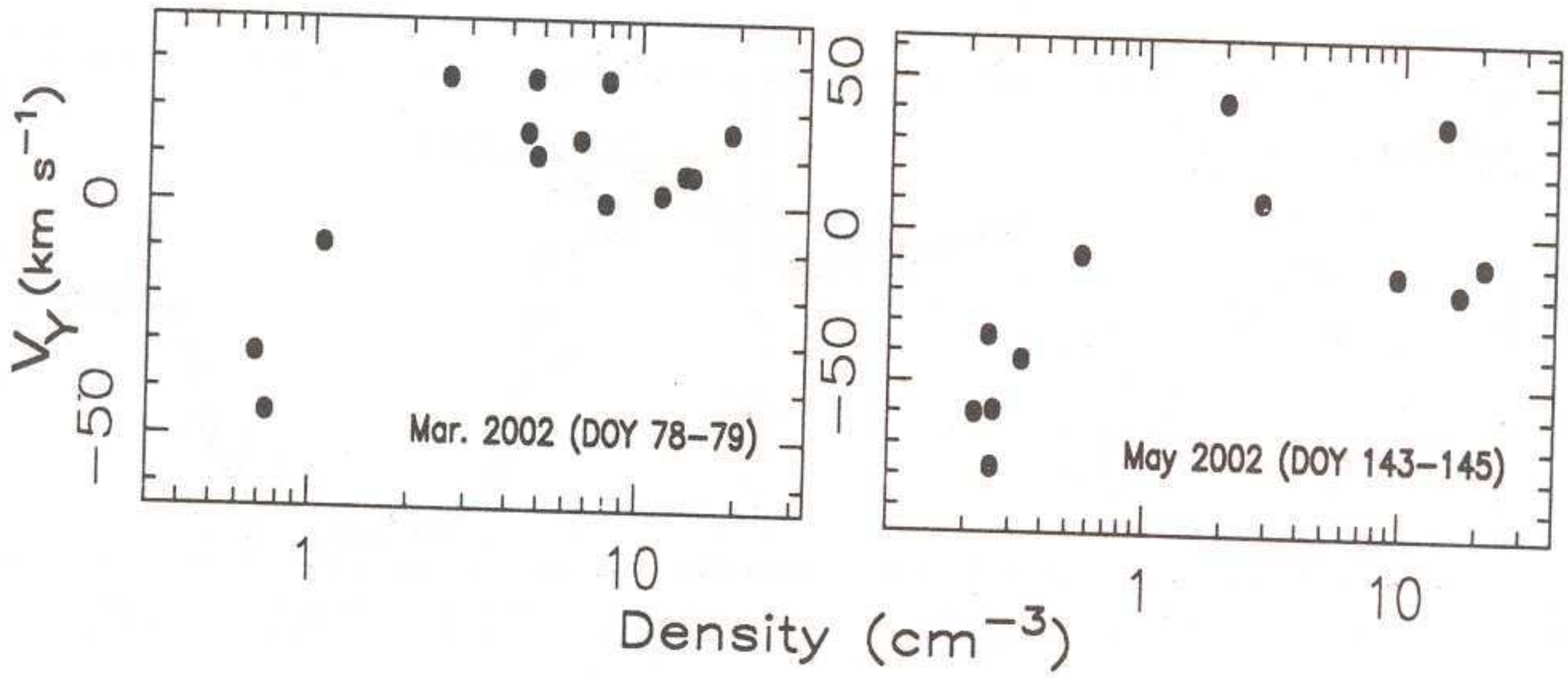

Figure 12: Plots hourly averages of the variation of proton density as a function of the azimuthal component of the solar wind velocity for the disappearance events of March 2002 (left panel) and May 2002 (right panel).

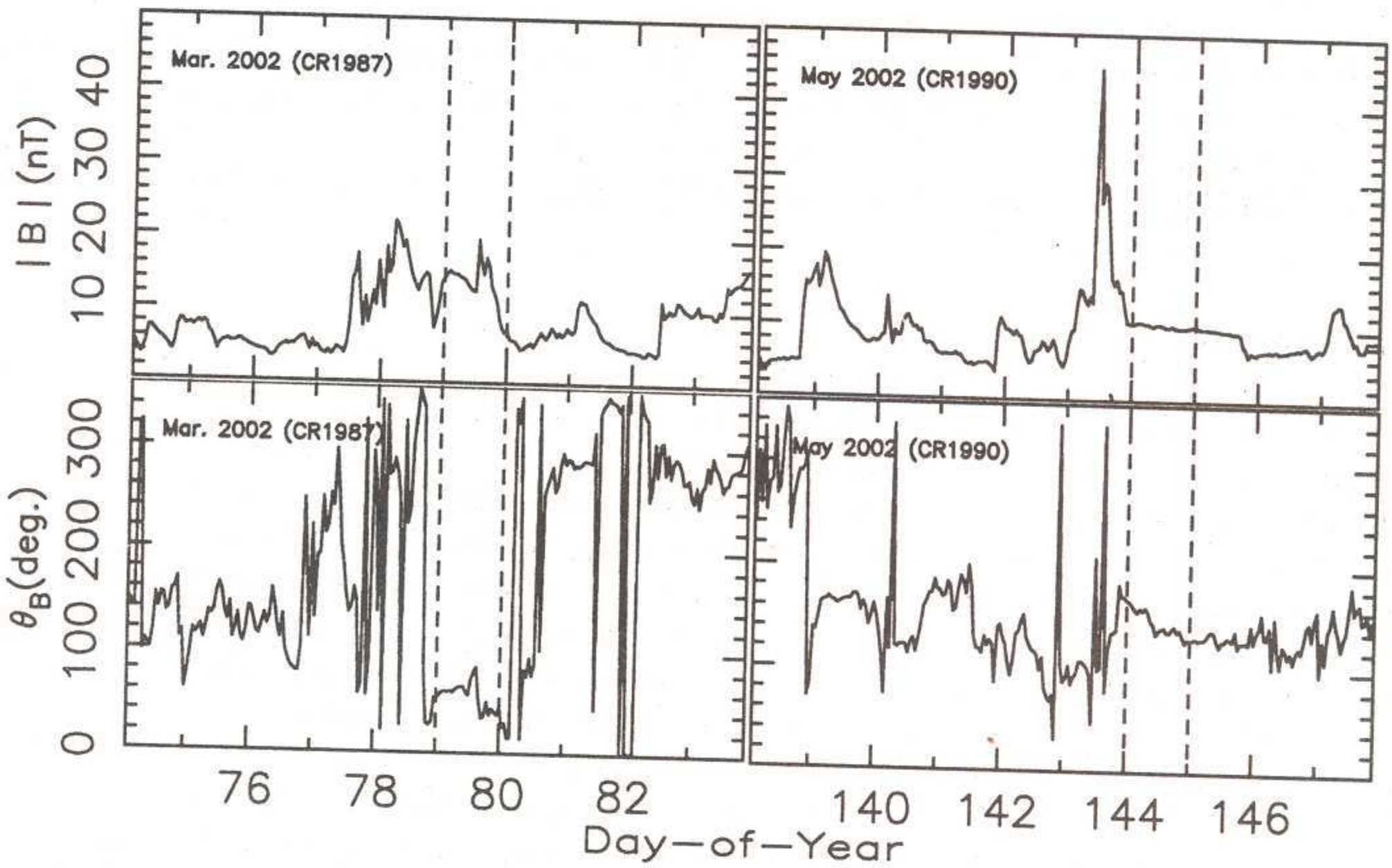

Figure 13: Shows the absolute magnitude of the IMF in nT and the actual direction of the IMF for the disappearance events of Mar 2002 (left upper and lower, respectively) and May 2002 (right upper and lower). The vertically oriented dashed parallel lines demarcate DOY 79 (left hand panels) and DOY 144 (right hand panels).

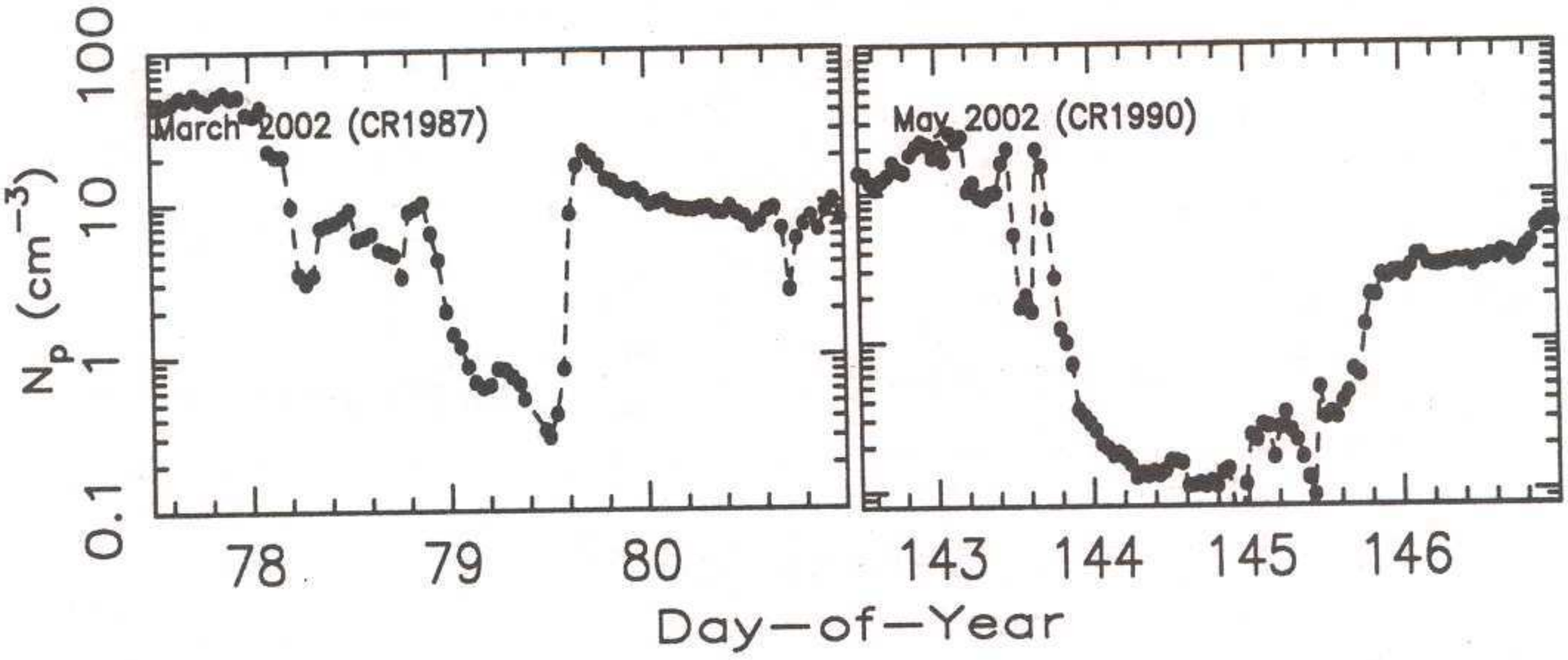

Figure 14: Plots hourly averages of ACE spacecraft measurements (at 1 AU) of proton density as a function of DOY for the March 2002 (left) and May 2002 (right).

stable and unipolar through the first half of DOY 79 for the event of March 2002 and the magnetic field is stable and unipolar during DOY 144, for the event of May 2002. Figure 14 shows by filled circles joined by a dashed line, hourly averages of ACE spacecraft measurements (at 1 AU) of proton density as a function of DOY for March 2002 (left panel), and May 2002 (right panel), respectively. It can be seen from Figure 14 that the densities remained low for about half a day during DOY 79 before beginning to rise again for the event of Mar 2002. For the May 2002 event, the densities remained low for the whole of DOY 144.

6 Discussion and conclusions

It has been argued [28] that the large magnetic flux expansion factors associated with the May 1999 event that took place during CR1949 and the small size of the coronal hole to which the solar wind flows were traced back could explain the low velocities seen. The extremely low densities observed, however, cannot be so easily explained. An interesting method for producing the low densities has been proposed by Janardhan et al. [28], by assuming that rearrangements in Coronal Hole boundaries would produce a pinch-off or separation of the solar wind outflow, thereby completely detaching the outflow from its solar source. The authors have then argued that if such a detached outflow occurred within 48 hours of its start and it continued to expand as it propagated out to 1 AU, an increase in its radius by a factor of 6-7 would lead to a decrease in densities by a factor of 200-300 at 1 AU. Thereby, typical particle densities of approximately 20-30 cm^{-3} at 0.5 AU could be reduced to 0.1 cm^{-3} at 1 AU given that the typical travel time between the Sun and the Earth, at these low velocities, is $\sim$5 days. In light of the arguments, it is interesting to ask if there could be any other candidates, apart from small mid-latitude coronal holes that could cause such low density, low velocity solar wind flows at 1 AU.

Apart from small mid-latitude coronal holes, another class of coronal holes is the so-called transient coronal holes (TCH), which were first discovered in Skylab data [33]. These TCH are short lived ($\sim$2 days) regions of dimmed X-ray intensity, which are sometimes observed in association

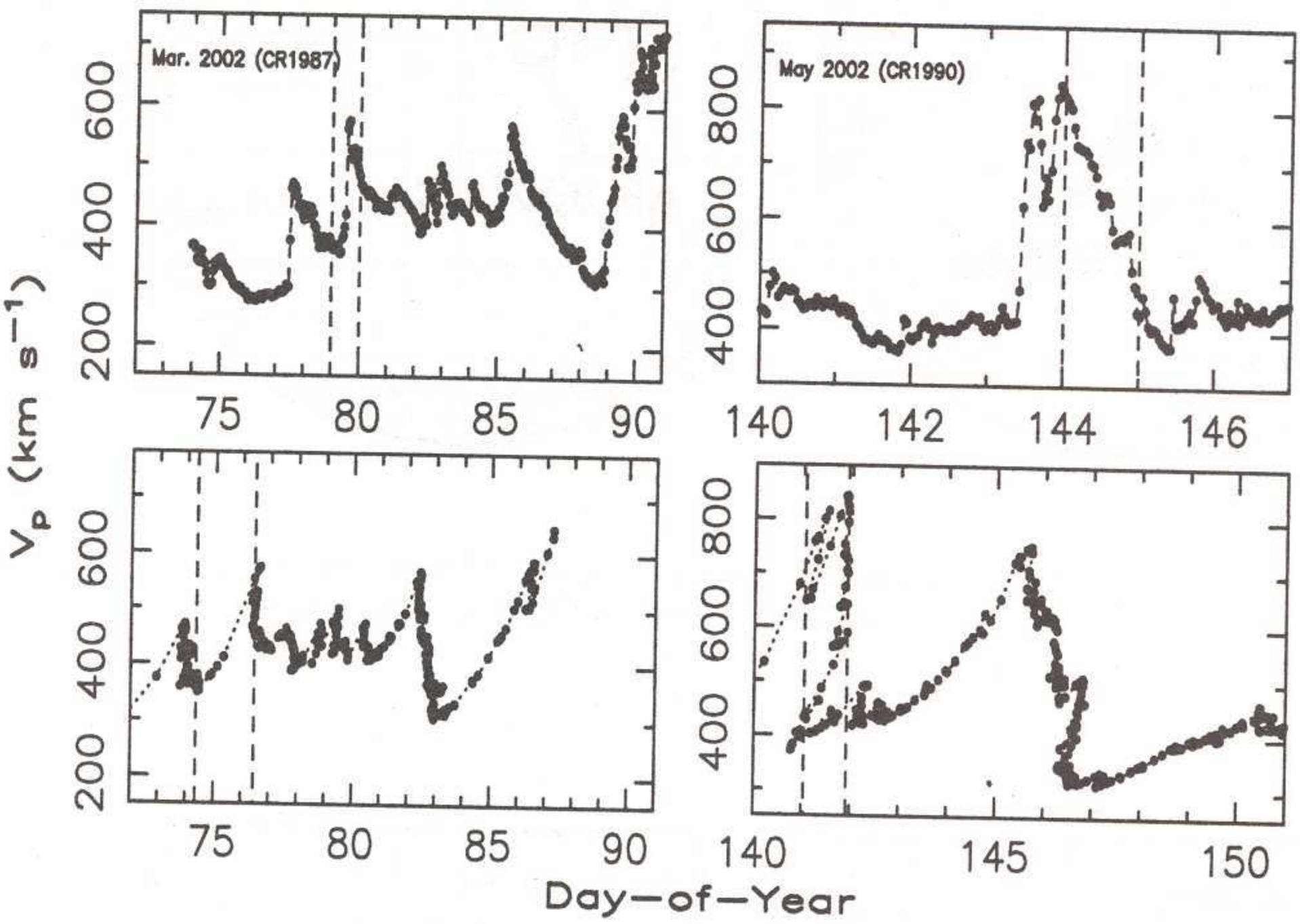

Figure 15: Shows hourly averages of solar wind velocities as observed by the SWEPAM instrument onboard the ACE spacecraft for the events of March 2002 (upper left) and May 2002 (upper right). The observed ACE velocities have been traced back to the source surface along Archimedean spirals from IAU to 2.5 $R_\odot$ and are shown for the March 2002 event (lower left) and May 2002 (lower right). The vertically oriented dashed parallel lines demarcate the event DOY (upper panels) and the corresponding traceback DOY (lower panels).

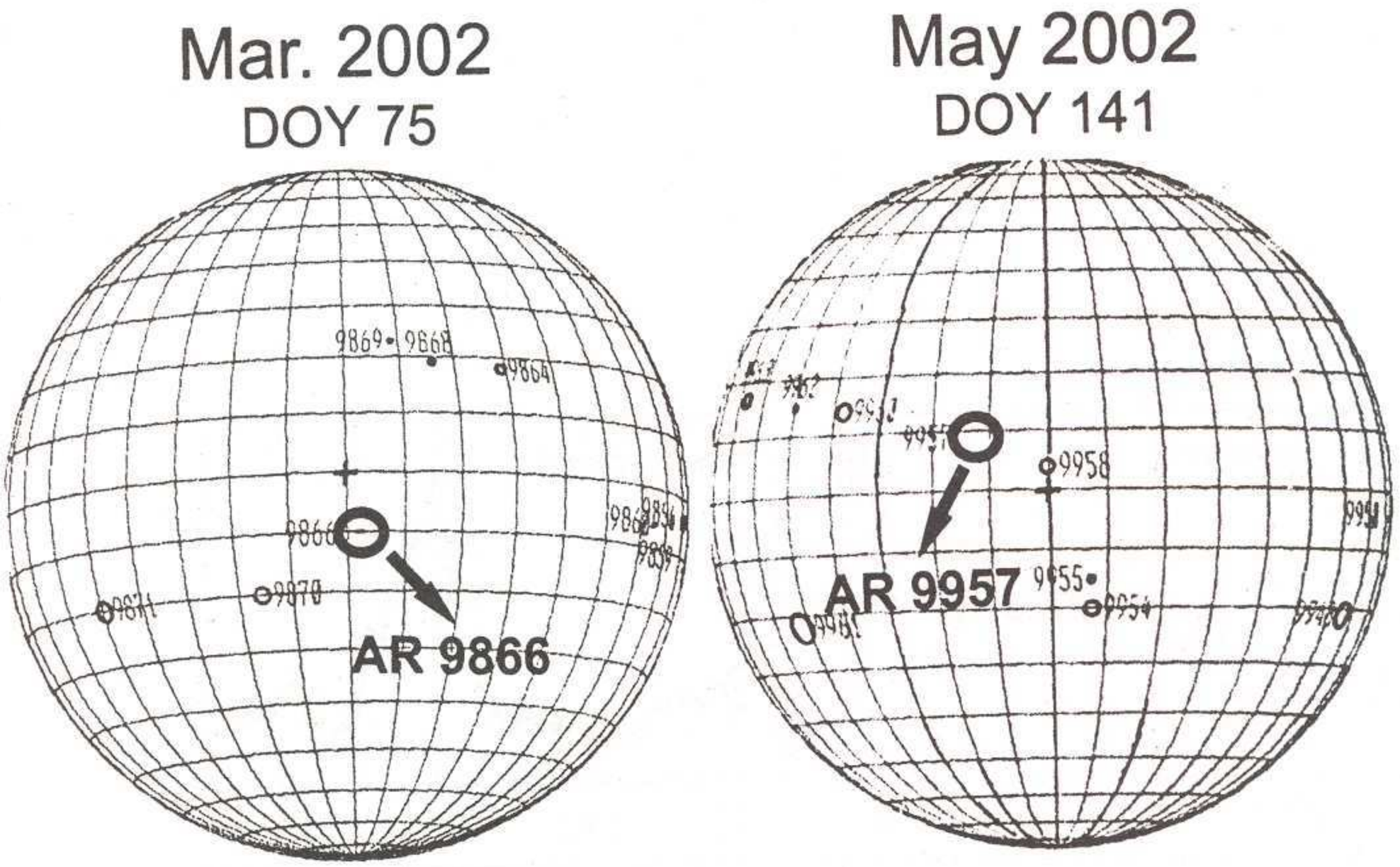

Figure 16: Maps of the solar photosphere on 16 March 2002 (left) and 21 May 2002 (right). The locations of the large active regions are shown with the locations of AR9866 and AR9957 being indicated by an arrow in the left and right panels, respectively.

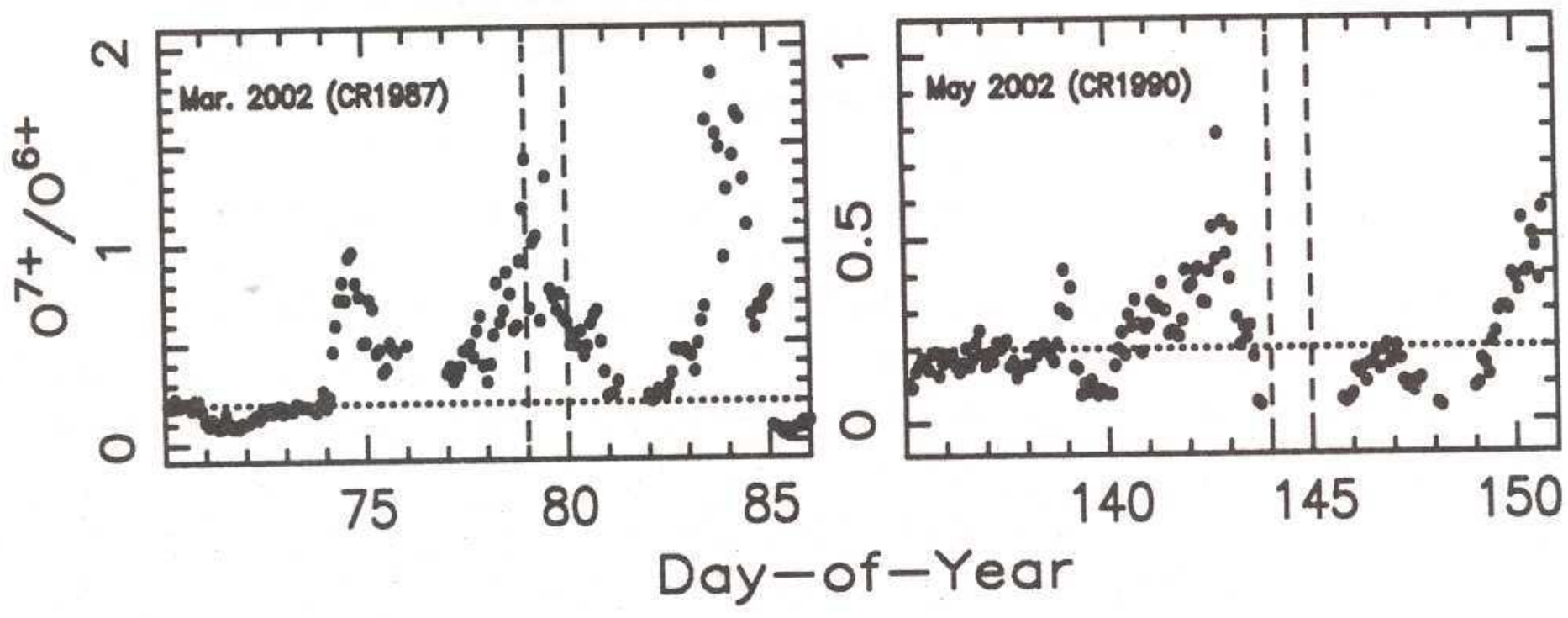

Figure 17: Shows as a function of DOY the charge state ratio O^{7+}/O^{6+} for the March 2002 event (left) and for the May 2002 event (right). The finely dotted horizontal line in both panels is marked at $O^{7+}/O^{6+} = 0.2$ while the vertically oriented parallel lines dermacate DOY 79 in March 2002 (left) and DOY 144 in May 2002 (right).

with CME's. In an extensive study of 19 TCH, using 9 years of data from the YOHKOH soft X-ray telescope (SXT), it has been shown [34] that TCH:

1. are small in size;
2. occur in magnetic unipolar regions trailing large active regions;
3. generally occur in regions where the magnetic neutral line shows large scale curvature; and
4. have short lifetimes, typically about 48 hours.

From the above it is clear that TCH could also be very good candidates for causing disappearance events. Their short lifetimes of $\sim$ 48 hours when compared with the typical travel times between the Sun and 1 AU of 3–5 days for the solar wind would imply that outflows originating at a small TCH can become totally disconnected from the source. However, the problem with detecting TCH is that the coronal radiation responsible for HeI 10830Å would come from higher altitudes than soft X-ray emission and thus represent large spatial scales. HeI 10830Å observations of coronal hole boundaries will therefore be blurred and cannot be used to detect the smallest TCH, which are generally small in size. Even at soft X-ray wavelengths, since the corona is optically thin, foreground and background emission can prevent the detection of TCH on the limb thereby limiting TCH detections to those that are well away from the limb. Thus, detecting TCH would require special and careful processing of soft X-ray and EUV data.

Figure 15 plots hourly averages of solar wind velocities as observed by the SWEPAM instrument onboard the ACE spacecraft for the events of March 2002 (upper left) and May 2002 (upper right). The observed ACE velocities have been traced back to the source surface at 2.5 $R_\odot$, using constant velocities along Archimedean spirals and are shown for the March 2002 event (lower right) and May 2002 (lower left). The vertically oriented dashed parallel lines demarcate the event DOY (upper panels) and the corresponding traceback DOY (lower panels). In a detailed study of the May 1999 event, it has been shown [28] that the source region was in the vicinity of the large active region complex AR8525 that was located at central meridian on 5 May 1999 when the low velocity solar wind flows began. The authors argued that the stable and unipolar nature of the flows from the vicinity of AR8525, the central meridian location of AR8525 taken together with the extensive and detailed work by Kahler and Hudson [34] described above, were indications that transient coronal holes could be an alternative solar source for explaining other such low velocity, tenuous solar wind flows seen at 1 AU. From Figure 10 (lower panel) we can see that the solar wind flows of 11 May 1999 originated from a small area on the Sun trailing AR8525 and the magnetic neutral line showed a large curvature. It is therefore not unreasonable to speculate that the other tenuous solar wind outflows listed in Table 1 could have probably originated in small TCH. The small area of the TCH associated with such an outflow would produce very low velocities as has been shown by several authors [35-38]. The typical lifetime of a TCH of $\sim$2 days as compared to solar wind travel time of $\sim$5 days would imply that the low velocity flow from the TCH would have been completely detached from the solar surface approximately three days before reaching 1 AU and after propagating roughly 40% of the distance to earth orbit. As described earlier, a simple expansion of this large detached low velocity flow region, as it propagated out to 1 AU, could give rise to an extremely low density cloud that engulfs the earth.

Active regions on the Sun are often ignored as a source for the IMF at 1 AU. However, it has been shown in a detailed theoretical study, complemented with a potential-field source-surface model for the coronal and inner-heliospheric magnetic fields, that solar wind outflows from active regions comprise $\leq$10% during solar minimum and up to 30–50% during solar maximum [39]. This finding stands inspite of the simplification that the authors made of a uniform, steady solar wind from the

source surface outward into the heliosphere. Figure 16 shows maps of the solar photosphere on 16 March 2002 (left panel) and 21 May 2002 (right panel).

Both the events were traced back using constant velocities along Archimedean spirals to the vicinity of AR9866 in March 2002 and AR9957 in May 2002. Both these active regions were located at central meridian. The locations of the large active regions are shown in Figure 16 and AR9866 and AR9957 have been emphasized and marked with a arrow in the left and right panels, respectively. It is instructive to note the correlation between the location of the active region at central meridian and the duration of the low velocities at 1 AU. From Figure 16 we can see that on DOY 141, when the low density solar wind flows began, AR9957 was located $\sim$12° East of the central meridian. Thus earth directed flows from this region would be of a longer duration as AR9957 would have been almost exactly at central meridian on DOY 142 and $\sim$12° to the west of central meridian on DOY 143. It is clear from Figure 14 that this is indeed the case with the duration of the May 2002 event being well over 24 hours as compared to the March 2002 event. For the March 2002 event, the source region in the vicinity of AR9866 is located a few degrees to the west of central meridian on DOY 75 when the low density flows began.

The right and left hand panels of Figure 17 shows the charge state ratio O^{7+}/O^{6+} for the events of March and May 2002, respectively. The finely dotted horizontal line in both panels is marked at $O^{7+}/O^{6+} = 0.2$ while the vertically oriented parallel lines demarcate DOY 79 in March 2002 (left panel) and DOY 144 in May 2002 (right panel). Unlike the May 1999 event the O^{7+}/O^{6+} ratio is above 0.2 during the two events, suggesting that the solar source was an active region open field [39].

From an analysis of the three disappearance events carried out it is apparent that stable and unipolar outflows from the Sun were responsible for all three events described. It is very interesting see p8 to note that the Alfvén radius in all events became independent of the magnetic field. From Figures 9 and 12 we can see that the azimuthal component of the solar wind velocity went as high as 100 km s^{-1} for the disappearance event of May 1999 and it went to $\sim$50 km s^{-1} for the two events of March 2002 and May 2002. If we therefore assume that this azimuthal velocity component (V_a) was due to co-rotation of the solar wind out to a distance corresponding to the Alfvén radius (R_A), then R_A can be computed since $R_A\Omega_\odot = V_a$, where, $\Omega_\odot = 1.642\times10^{-4}$ deg s^{-1} is the angular speed of the Sun. Thus R_A could extend outward from its normal location of $\sim$0.05 AU to as much as 0.23 AU for the May 1999 event and out to 0.11 AU for the two events in March and May 2002. Thus R_A can extend outward by a factor of 2–5 during a disappearance event.

In conclusion we can say that this work has highlighted the role of stable and unipolar outflows from the Sun, possibly from coronal holes or active region open fields, that are responsible for all three events studied. The work has also highlighted the need for systematic studies of the dynamics and evolution of CH boundaries. Such studies could help define coronal hole boundary structure and thereby help in understanding boundary field connectivities. Regular and systematic observations by both ground and space based platforms will be required to identify many more such events and ground based IPS observations will be of great value in such future studies.

Acknowledgment: This work is supported by the Department of Space, Government of India. The authors would like to thank the staff of the Radio Astronomy Center, Ooty (Udhagamandalam), India and the staff of the Solar Terrestrial Environment Laboratory, Toyokawa, Japan.

References

1 Hewish A, Scott PF, Wills D, *Nature*, 203 (1964) 1214.

2 Dennison PA, Hewish A, *Nature*, 213 (1967) 343.
3 Scott SL, Coles WA, Bourgois G, *Astron. Astrophys.*, 123 (1983) 207.
4 Coles, WA, Rickett BJ, Rumsey VH, Kaufman JJ, Turley DG, Ananthakrishnan S, Armstrong JW, Harmon JK, Scott SL, *Nature,* 286 (1980) 239.
5 Rickett BJ, Coles WA, *J. Geophys.Res.*, 96 (1991) 1717.
6 Manoharan PK, *Sol. Phys.* , 148 (1993) 153.
7 Tokumaru M, Kojima M, Fujiki K, Yamashita M, Baba D, *J. Geophys.Res.*, 110 (2005) A01109.
8 Hewish A, Tappin SJ, Gapper GR, *Nature*, 314 (1985) 137.
9 Hewish A,Bravo S, *Sol. Phys.*, 106 (1986) 185.
10 Janardhan P, Balasubramanian V, Ananthakrishnan S,*Proc. of the 31st. ESLAB Symp., ESA SP-415* (1997) 177.
11 Balasubramanian V, Janardhan P, Ananthakrishnan S, Manoharan PK, *Bull. Astr. Soc. India*, 21 (1993) 469.
12 Janardhan P, Balasubramanian V, Ananthakrishnan S, Dryer M, Bhatnagar A, McIntosh PS, *Sol. Phys.*, 166 (1996) 379.
13 Balasubramanian V, Janardhan P, Ananthakrishnan S, Srivatsan R, *Bull. Astr. Soc. India,* 24 (1996) 829.
14 Smart DF, Shea MA, *J. Geophys.Res.*, 90 (1985) 183.
15 Ananthakrishnan S, Kojima M, Tokumaru M, Balasubramanian S, Manoharan PK, Dryer M, *Proc. of Solar Wind 9 Conf., S.R. Habbal, eds., AIP, New York.*, (1999) 321.
16 Ananthakrishnan S, Tokumaru M, Kojima M, *Adv. Space Res.*, 29 (2002) 1467.
17 Tyler GL, Vesecky JF, Plume MA, Howard HT, Barnes A, *Astrophys. J.*, 249 (1981) 318.
18 Manoharan PK, Ananthakrishnan S, *Mon. Not. Royal Astron. Soc.*, 244 (1990) 691.
19 Marians M, *Radio Sci.*, 10 (1975) 115.
20 Gosling JT, Asbridge JR, Bame, SJ, Feldman WC, Zwickl RG, Pashmann G, Sckopke N,Russell CT, *J. Geophys.Res.*, 87 (1982) 239.
21 Schwenn R, *Solar Wind 5, NASA Conf. Pub. 2280, M. Neugebauer (ed.),* (1982) 489.
22 Crooker NU, Shodhan S, Gosling JT, Simmerer J, Lepping RP, Steinberg JT, Kahler SW, *Geophys. Res. Lett.*, 27 (2000) 3769.
23 Farrugia CJ, Singer HJ, Evans D, Berdichevsky D, Scudder JD, Ogilvie KW, Fitzenreiter RJ, Russell CT, *Geophys. Res. Lett.*, 27 3773.
24 Richardson IG, Berdichevsky D, Desch MD, Farrugia GJ, *Geophys. Res. Lett.*, 27 (2000) 3761.
25 Usmanov AV, Goldstien ML, Farrell WM, *Geophys. Res. Lett.*, 27 (2000) 3765.
26 Vats HO, Sawant HS, Oza R, Iyer KN, Jadhav R, *J. Geophys.Res.*, 106 (2001) 25121.
27 Balasubramanian V, Janardhan P, Srinivasan S, Ananthakrishnan S, *J. Geophys.Res.*, 108 (2003) 1121.
28 Janardhan P, Fujiki K, Kojima M, Tokumaru M, Hakamada K, *J. Geophys.Res.*, 110 (2005) A08101.
29 Usmanov AV, Farrell WM, Ogilvie KW, Goldstien ML, *Proc. EGS-AGU-EUG Joint Assembly,* (2003).
30 Ananthakrishnan S, Coles WA, Kaufman J, *J. Geophys.Res.*, 85 (1980) A116025.
31 Hakamada K, Kojima M, *Sol. Phys.* , 187 (2005) 115.
32 Liewer PC, Neugebauer M, Zurbuchen T, *Sol. Phys.* , 223 (2004) 209.
33 Rust DM, *Space Sci. Rev.*, 34 (1983) 21.
34 Kahler SW, Hudson HS, *J. Geophys.Res.*, 106 (2001) 29239.
35 Wang, Y-M, Sheeley Jr., *Astrophys. J.*, 355 (1990) 726.
36 Sheeley NR Jr., Swanson ET, Wang Y-M, *J. Geophys.Res.*, 96 (1991) 13861.
37 Nolte JT, Krieger AS, Timothy AF, Gold RE, Roelof EC, Vaiana G, Lazarus AJ, Sullivan JD, McIntosh PS, *Sol. Phys.* , 46 (1976) 303.

38 Neugebauer M, Forsyth RJ, Galvin AB, Harvey KL, Hoeksema JT, Lazarus AJ, Lepping RP, Linker JA, Mikic Z, Steinberg JT, von Steiger R, Wang Y-M, Wimmer-Schweingruber RF, *J. Geophys.Res.*, 103 (1998) 14587.
39 Schrijver CJ, Derosa ML, *Sol. Phys.*, 212 (2003) 165.

[*Received: 05.01.07; accepted: 15.03.07*]